JACS
JOURNAL OF THE AMERICAN CHEMICAL SOCIETY

ARTICLE

pubs.acs.org/JACS

Molecular Packing of High-Mobility Diketo Pyrrolo-Pyrrole Polymer Semiconductors with Branched Alkyl Side Chains

Xinran Zhang,[†] Lee J. Richter,[‡] Dean M. DeLongchamp,*[,†] R. Joseph Kline,[†] Matthew R. Hammond,[†] Iain McCulloch,*[,∥] Martin Heeney,[∥] Raja S. Ashraf,[∥] Jeremy N. Smith,[⊥] Thomas D. Anthopoulos,[⊥] Bob Schroeder,[#] Yves H. Geerts,[#] Daniel A. Fischer,[§] and Michael F. Toney[▽]

[†]Polymers Division, [‡]Surface and Microanalysis Science Division, and [§]Ceramics Division, National Institute of Standards and Technology, Gaithersburg, Maryland 20899, United States

[∥]Department of Chemistry and Centre for Plastic Electronics, and [⊥]Department of Physics and Centre for Plastic Electronics, Imperial College London, South Kensington, SW7 2AZ, United Kingdom

[#]Université Libre de Bruxelles (ULB), Faculté des Sciences, Laboratoire Chimie des Polymères, CP 206/1, Boulevard du Triomphe, 1050 Brussels, Belgium

[▽]Stanford Synchrotron Radiation Lightsource, Menlo Park, California 94025, United States

Supporting Information

ABSTRACT: We describe a series of highly soluble diketo pyrrolo-pyrrole (DPP)-bithiophene copolymers exhibiting field effect hole mobilities up to 0.74 $cm^2\ V^{-1}\ s^{-1}$, with a common synthetic motif of bulky 2-octyldodecyl side groups on the conjugated backbone. Spectroscopy, diffraction, and microscopy measurements reveal a transition in molecular packing behavior from a preferentially edge-on orientation of the conjugated plane to a preferentially face-on orientation as the attachment density of the side chains increases. Thermal annealing generally reduces both the face-on population and the misoriented edge-on domains. The highest hole mobilities of this series were obtained from edge-on molecular packing and in-plane liquid-crystalline texture, but films with a bimodal orientation distribution and no discernible in-plane texture exhibited surprisingly comparable mobilities. The high hole mobility may therefore arise from the molecular packing feature common to the entire polymer series: backbones that are strictly oriented parallel to the substrate plane and coplanar with other backbones in the same layer.

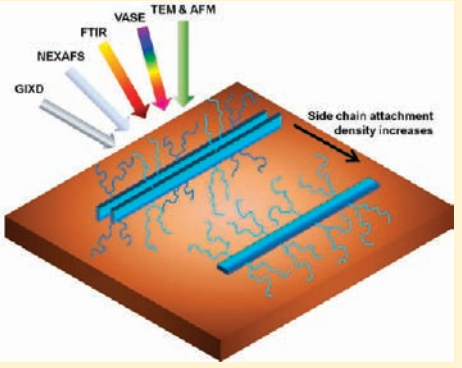

INTRODUCTION

The past decade has witnessed a rapid expansion in the number of solution-processable polymer semiconductors that can exhibit field-effect mobilities (μ) exceeding 0.1 $cm^2\ V^{-1}\ s^{-1}$ and compete with the performance of amorphous silicon.[1−23] This progress has made polymer semiconductors a promising candidate semiconducting layer for low-cost flexible thin film transistors (TFTs) to enable large-area electronics applications such as display backplanes[24] and radio frequency identification (RFID) tags.[25]

Significant effort has been invested in deriving structure−property relationships for high-mobility polymer semiconductors. Polymers within the largest family of polymer semiconductors, the polythiophene derivatives, typically exhibit a lamellar packing motif with π-stacked conjugated backbones separated by lamellae of insulating alkyl side chains.[1−4] Early studies of poly(3-hexylthiophene) (P3HT)[1] proposed that it is essential that the π-stacking direction lie in the substrate plane, making the common ring plane of the backbone "edge-on" upon the substrate. This molecular packing behavior orients what are thought to be the two fast transport directions (along the backbone and $\pi-\pi$ stacking) within the substrate plane for conventional TFT geometries. Both poly(3,3′-dialkyl-quaterthiophene) (PQT)[2] and poly(2,5-bis(3-alkylthiophen-2-yl)thieno[3,2-b]-thiophene) (PBTTT)[3] exhibit a similar structure. In the case of PBTTT,[26] a low linear side chain attachment density led to formation of a highly ordered structure that permitted side chain interdigitation and alkane crystallization between adjacent backbone layers. The PBTTT synthetic design of low attachment density and linear side chains, however, sacrificed room-temperature solubility. PBTTT therefore required elevated temperatures[3] or uncommon solvents[27] for solution processing.

Recent reports have shown that high-mobility polymer semiconductors ($\mu \approx 0.2$ $cm^2\ V^{-1}\ s^{-1}$ or even higher) are feasible with a face-on alignment of the backbone ring planes with an out-of-plane $\pi-\pi$ stacking direction,[11,12,19] despite the placement of insulating alkyl chains in the plane of 2D charge transport.

Received: May 25, 2011
Published: August 04, 2011

Scheme 1. Synthetic Routes to the DPPT Polymers

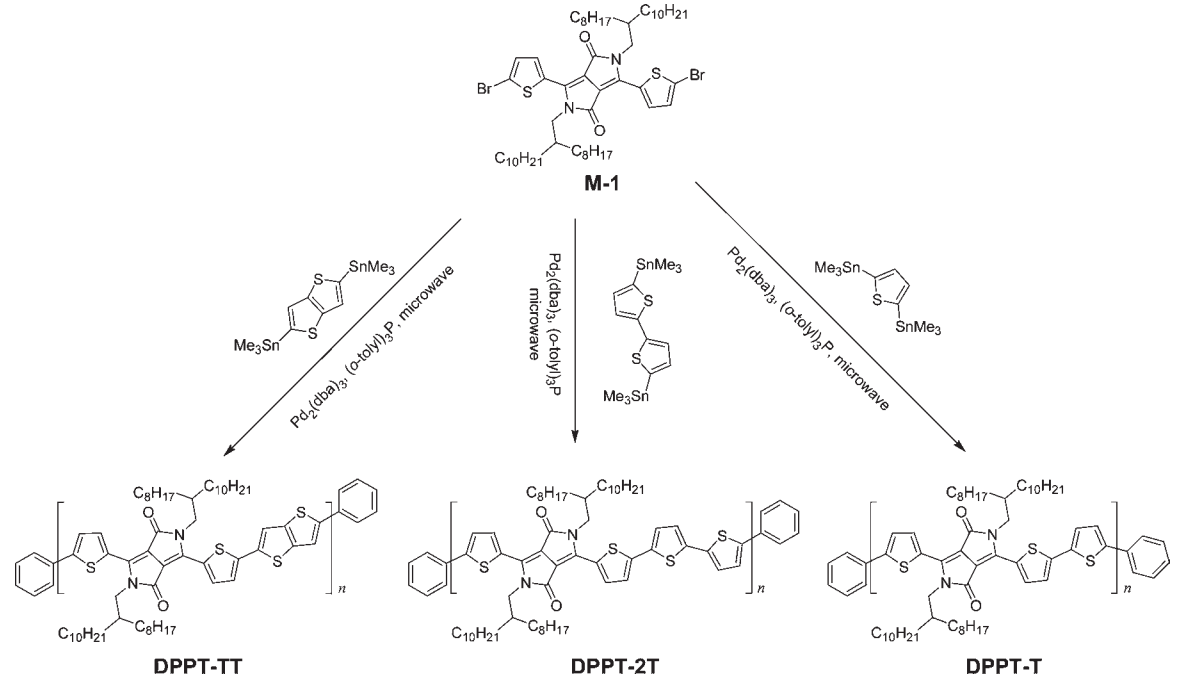

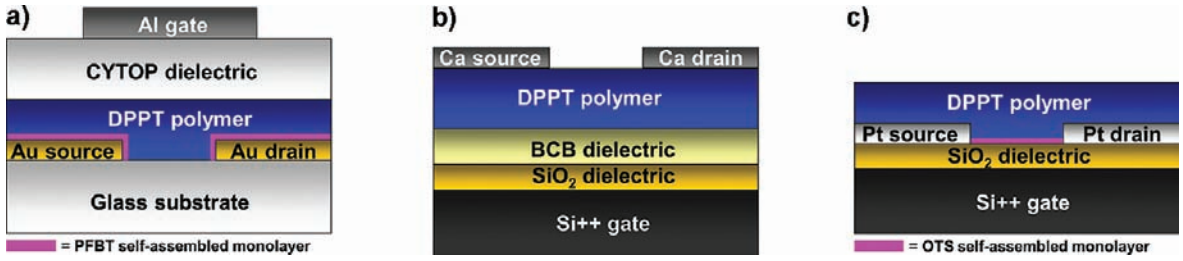

Figure 1. Device structures of (a) TGBC; (b) BGTC; and (c) BGBC OTFTs. PFBT and OTS refer to pentafluorobenzenethiol and octyltrichlorosilane, respectively.

Two striking examples of this molecular packing behavior were a naphthlenedicarboximide–bithiophene copolymer (P(NDI2OD-T2)) reported by Yan et al. ($\mu \approx 0.45$–0.85 cm^2 V^{-1} s^{-1})[11,12] and an indacenodithiophene–benzothiadiazole copolymer (IDT-BT) reported by Zhang et al. ($\mu \approx 1$ cm^2 V^{-1} s^{-1}).[19] It is also worth noting that, unlike the case of PBTTT, the high charge mobilites of P(NDI2OD-T2) and IDT-BT were accompanied by excellent room-temperature solubility in common organic solvents, due to the incorporation of long branched alkyl side chains that were previously thought to be detrimental to charge transport.[10,16,17] These solubilizing groups make the polymers more compatible with large-area roll-to-roll production processes.[28–30] Two questions naturally arise from this discussion: (1) Beyond the edge-on/face-on orientation of conjugated backbone, is there a more essential structural characteristic responsible for high mobilities in polymer semiconductors? (2) In the presence of disordered, bulky side chains, how do the conjugated backbones pack to enable effective charge transport?

In this Article, we characterize the thin film molecular packing behavior of three thiophene-based donor–acceptor copolymers containing electron-deficient diketo pyrrolo-pyrrole (DPP) units with pendant 2-octyldodecyl groups. The repeat units of these polymers consist of two moieties: (1) a common DPP-bithiophene moiety and (2) a variable moiety that can be thienothiophene (TT), bithiophene (2T), or monothiophene (T). The corresponding polymers are hereafter referred to as DPPT-TT, DPPT-2T, and DPPT-T, respectively, and are depicted in Scheme 1. These polymers are highly soluble in common organic solvents such as chloroform and chlorobenzene at room temperature, yet they can exhibit high field-effect mobilities comparable to those of the best-performing polymer semiconductors with linear side chains. Several aspects of molecular packing behavior, such as the orientation of conjugated backbones, the side chain arrangement, and the in-plane texture, provide new insights into structure–property relationships for high-mobility polymer semiconductors with branched side chains.

RESULTS

OTFT Device Performance. Top gate bottom contact (TGBC) devices with Au source/drain electrodes (Figure 1a) were fabricated to evaluate the charge carrier mobilities of the DPPT polymers. In devices with relatively long channels (L = 50 μm; channel width, W = 500 μm), high saturation/linear hole

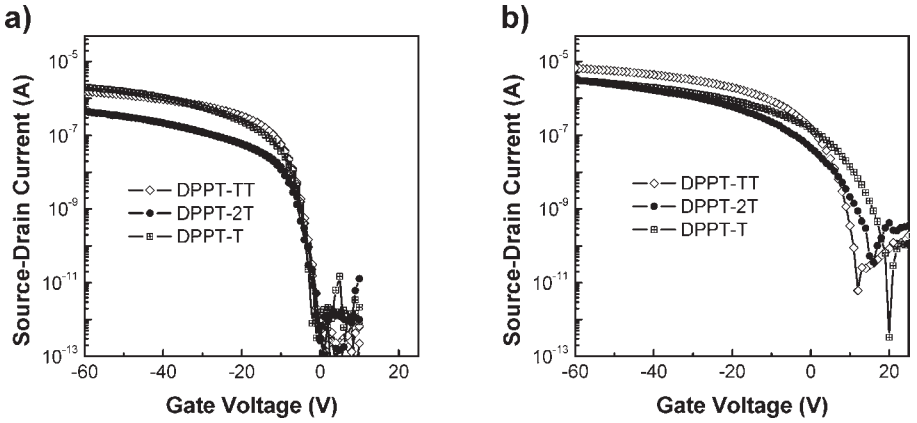

Figure 2. Typical transfer curves of (a) TGBC (L = 50 μm and W = 500 μm) and (b) BGBC (L = 10 μm and W = 1000 μm) OTFT devices. The drain voltage used in measuring TGBC devices was −6 V for DPPT-TT and −5 V for DPPT-2T and DPPT-T, respectively. The drain voltage used in measuring BGBC devices was −2 V for all three polymers. Standard uncertainty in measuring on-current is within ±1%.

Table 1. OTFT Properties of the DPPT Polymers Measured in TGBC and BGTC Devices

	TGBC devices				BGTC devices			
polymer	μ_{sat} ($cm^2\ V^{-1}\ s^{-1}$)[a]	μ_{lin} ($cm^2\ V^{-1}\ s^{-1}$)	V_T (V)	on/off ratio (linear)	μ_{sat} ($cm^2\ V^{-1}\ s^{-1}$)	μ_{lin} ($cm^2\ V^{-1}\ s^{-1}$)	V_T (V)	on/off ratio (linear)
DPPT-TT	0.38 ± 0.05	0.20 ± 0.05	−10 ± 3	10^7	(1.5 ± 0.2) × 10^{-3}	(1.2 ± 0.2) × 10^{-3}	5 ± 1	10^4
DPPT-2T	0.2 ± 0.1	0.05 ± 0.02	−5 ± 2	10^5−10^6				
DPPT-T	0.6 ± 0.1	0.3 ± 0.1	−5 ± 2	10^6	(1.2 ± 0.1) × 10^{-2}	(0.6 ± 0.1) × 10^{-2}	6.5 ± 0.1	10^3−10^4

[a] Each mobility or threshold voltage value represents the average from at least three devices on a single chip, with an error bar denoting the standard deviation.

mobilities (μ_{sat}) were found. Specifically, 0.38/0.20, 0.20/0.05, and 0.60/0.30 $cm^2\ V^{-1}\ s^{-1}$ were obtained from DPPT-TT, DPPT-2T, and DPPT-T, respectively. The on/off ratios are on the order of ≈10^6, and threshold voltages are all reasonably low (Figure 2 and Table 1). We note that the highest mobility obtained from DPPT-T might be ascribed to its high molecular mass (M_n = 104 kDa) which is often thought to be beneficial for polymer-based OTFTs due to enhanced intergrain connection.[14,31] It is reasonable to expect enhanced mobilities from DPPT-TT and DPPT-2T provided that higher molecular masses can be achieved. Indeed, Li et al. reported a mobility of 0.94 $cm^2\ V^{-1}\ s^{-1}$ from TGBC devices based on DPPT-TT with a comparably high molecular mass (M_n = 90 kDa).[20] It appeared that electron transport was also present in spite of using Au electrodes (work function ≈ 5.1 eV). To reliably estimate electron mobilities, bottom gate top contact (BGTC) devices with Ca (work function ≈ 2.9 eV) source/drain electrodes (Figure 1b) were used. The measured μ_{sat} values in devices with L = 40 μm and W = 1000 μm were 1 or 2 orders of magnitude lower than the corresponding hole mobilities (see Table 1, as well as Figure S1 in the Supporting Information).

Since the ionization potentials of all three polymers (Table 2) are higher than the work function of Au, hole injection barriers are likely to be non-negligible. The mobilities in our Au-based devices, especially those with short channels (≤10 μm), may be underestimated as a result of the presence of significant contact resistance. This effect is likely the origin of the differences between linear and saturation mobilities. In view of such contact effects, bottom gate bottom contact (BGBC) devices with Pt (work function ≈ 5.65 eV) source/drain electrodes (Figure 1c) were used to give a more reasonable evaluation of the channel length dependence of μ_{sat}.[32] As seen from Figure 3b and c, the mobilities of DPPT-2T and DPPT-T decrease significantly as channel length increases (field strength decreases), suggesting field-assisted charge transport. In contrast, the mobilities of DPPT-TT only show weak dependence on channel length (Figure 3a), which could indicate field independent transport and good contacts. However, as DPPT-TT has the highest ionization potential among the three polymers, it is likely that field-assisted transport is masked by contact effects in these devices. A detailed analysis of contact resistance will not be included here, as our focus is to correlate charge mobility to molecular packing behavior. It is noteworthy that annealing at 150 °C for 5 min improved μ_{sat} of all the Pt-based devices by a factor of ≈1.5−2. Hole mobilities of ≈0.4 $cm^2\ V^{-1}\ s^{-1}$ or even higher were measured from annealed short-channel devices (L = 5 μm) for

Table 2. Ionization Potential (IP) Values and Ultraviolet−Visible−near Infrared (UV−vis−NIR) Absorption Peak Positions for the DPPT Polymers

		λ_{max} (nm)		
polymer	IP (eV)	solution	as-cast film	annealed film
DPPT-TT	5.4	793	814	816
DPPT-2T	5.25	775	787	790
DPPT-T	5.2	801	819	827

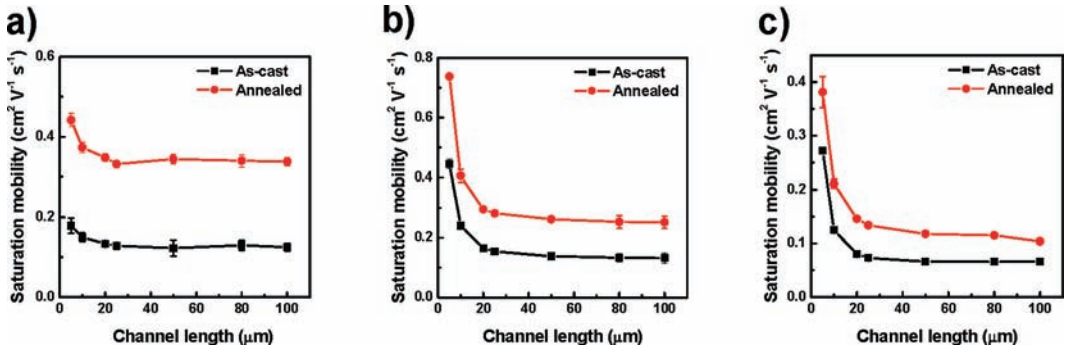

Figure 3. Channel length dependence of saturation regime mobilities for (a) DPPT-TT; (b) DPPT-2T; and (c) DPPT-T BGBC OTFT devices with Pt source/drain electrodes. Each data point in the $\mu_{sat}-L$ plots represents the average mobility of five devices, with an error bar denoting the standard deviation. The linear regression between −60 and −40 V of each $I_D^{1/2}$ vs V_G transfer curve is used for the mobility calculation.

all three polymers, with 0.74 $cm^2\ V^{-1}\ s^{-1}$ being the highest (DPPT-2T). In the case of long-channel devices ($L \geq 50\ \mu m$), high μ_{sat} values of ≈0.35, ≈0.25, and ≈0.10 $cm^2\ V^{-1}\ s^{-1}$ were obtained from DPPT-TT, DPPT-2T, and DPPT-T, respectively.

Characterization of Molecular Packing Behavior. Spectroscopy, diffraction, and microscopy measurements will be described only for DPPT polymer films cast from chloroform (on OTS), to match the conditions of our BGBC devices. The effect of casting solvent was determined to be insignificant as suggested by the comparison between TGBC and BGBC devices (cast from chlorobenzene and chloroform, respectively, vide supra), and will not be addressed in this Article.

Grazing-Incidence X-ray Diffraction (GIXD). GIXD has been widely used as an effective way to identify molecular packing behaviors in organic thin films.[5,12,14,15,31,33,34] With a two-dimensional (2D) detector for fiber-textured films (no in-plane crystallographic orientation), a diffraction pattern is captured with information in both out-of-plane (q_z) and in-plane ($q_{x,y}$) spacings. For a spin-cast polymer film with a lamellar packing motif, if the lamellar stacking direction, or (100) direction, is oriented parallel to the substrate surface normal, (h00) diffraction peaks corresponding to the lamellar spacing will be observed along q_z, and those related to the smaller backbone repeat unit and lateral molecular spacings, that is, (0k0) and (00l), will appear at large $q_{x,y}$, often near the $q_{x,y}$ axis. In the case that the (100) direction is highly oriented parallel to the substrate surface, the (h00) and (0k0) peaks will appear in directions orthogonal to this, that is, (h00) peaks along $q_{x,y}$ while (0k0) near the meridian (nominally q_z). The shape of the diffraction peaks can be used to infer how well the polymer crystals are oriented. Typically, highly oriented films exhibit diffraction patterns with elliptical spots, while those containing a significant amount of tilted or misoriented crystallites exhibit arcs at constant q.

The GIXD patterns acquired from DPPT-TT and DPPT-2T films (Figure 4a,b) were very similar, indicating lamellar packing parallel to the surface normal with an edge-on (100) orientation of the conjugated plane, similar to most reported high-mobility polymer semiconductors such as PBTTT.[33] The as-cast DPPT-TT and DPPT-2T films contained significant populations of crystallites with tilted (100) orientations as well as a small fraction of face-on domains, as suggested by the arc shape of the (h00) and (010) peaks and the appearance of weak (100) peaks along $q_{x,y}$ and (010) peaks along the meridian (approximately q_z). In contrast, the annealed DPPT-TT and DPPT-2T films were composed of highly oriented edge-on domains and negligible face-on domains, as inferred from the elliptical patterns with the decreased intensities of (100) peaks along $q_{x,y}$ and (010) peaks near q_z. The (010) peaks from both polymers showed a streaklike appearance, suggesting the lack of registry between adjacent lamellae. Table S1 in the Supporting Information lists all diffraction peak positions and the calculated d-spacings. The d-spacings for DPPT-TT and DPPT-2T were identical within experimental error: lamellar spacing ≈2.0 nm and $\pi-\pi$ stacking distance of ≈0.38 nm, irrespective of thermal history.

The GIXD pattern acquired from an as-cast DPPT-T film (Figure 4c) was remarkably different from those of DPPT-TT and DPPT-2T. Specifically, a preferentially face-on backbone orientation was found, as seen from the strong (010) peak along the meridian. The domains also appeared less ordered compared to as-cast DPPT-TT and DPPT-2T films, judging from the lack of high-order (h00) peaks and the broader peak widths. After thermal annealing, however, the fraction of face-on domains was greatly reduced, leading to a diffraction pattern showing a bimodal orientation distribution of edge-on and face-on domains. In addition, the peaks sharpened, showing improved order. The lamellar spacing and $\pi-\pi$ stacking distance were 2.1 and 0.38 nm, respectively, regardless of thermal history and orientation. For all three polymers, a diffuse ring which might come from the disordered alkyl chains[35] was observed in all diffraction patterns, and the diffraction peaks associated with the backbone repeat units, namely, the (00l), were not detected.

Near-Edge X-ray Absorption Fine Structure (NEXAFS) Spectroscopy. NEXAFS spectroscopy[36] is an element-specific, bond-sensitive technique which probes ≈6 nm into the sample/air interface in its partial electron yield (PEY) mode. Average conjugated plane (π^* orbital) orientation in polymer semiconductors can be determined by collecting carbon K-edge spectra with multiple incident angles of the linearly polarized soft X-rays,[4,34,37] as the 1s → π^* intensity is proportional to the squared dot product of the incident electric field vector and the vector normal to the conjugated plane of the backbone. The angular dependence of the 1s → π^* intensities is usually expressed by a dichroic ratio, R, which is the difference between the extrapolated intensities at 90° and 0° incidence, divided by their sum.[4,37] The R values calculated from the 1s → π^* intensities can vary from ≈0.7 (reduced from 1.0 by the finite polarization purity of the radiation source), corresponding to fully edge-on aromatic rings, to −1.0, corresponding to fully face-on aromatic rings. A more positive R signifies a larger average tilting angle of the transition dipole away from the substrate. The side-chain orientation is

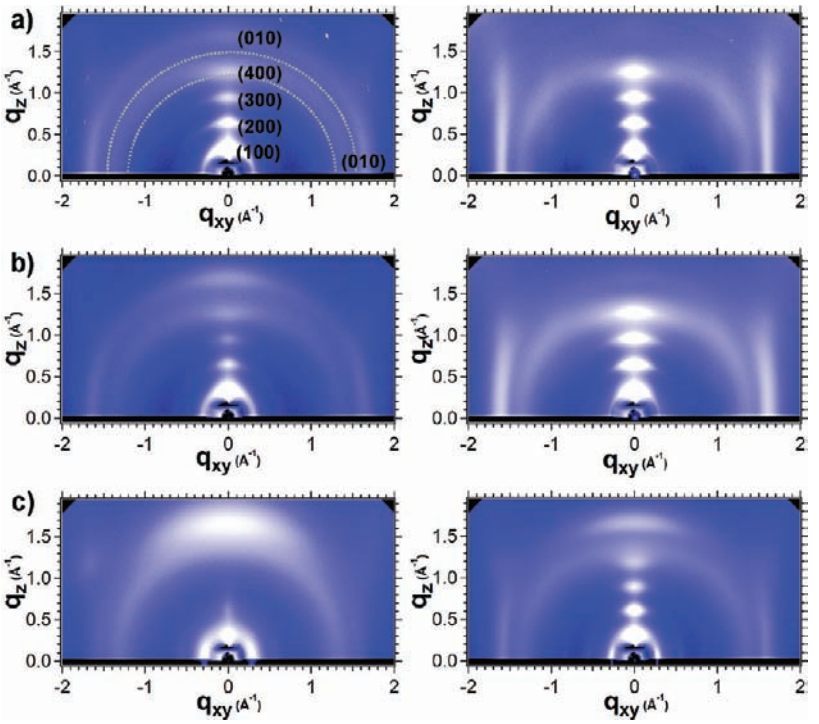

Figure 4. Two-dimensional grazing incidence X-ray diffraction (GIXD) from thin films of (a) DPPT-TT; (b) DPPT-2T; and (c) DPPT-T. The images in the left column were acquired from as-cast films, while those in the right column from annealed films. Due to the GIXD geometry, the meridian of the images ($q_{x,y} = 0$) does not correspond to a specular condition. The two dotted gray arcs in (a) are guides to the eye, highlighting the diffuse ring possibly arising from disordered alkyl side chains. Similar diffuse rings can be found in all other images.

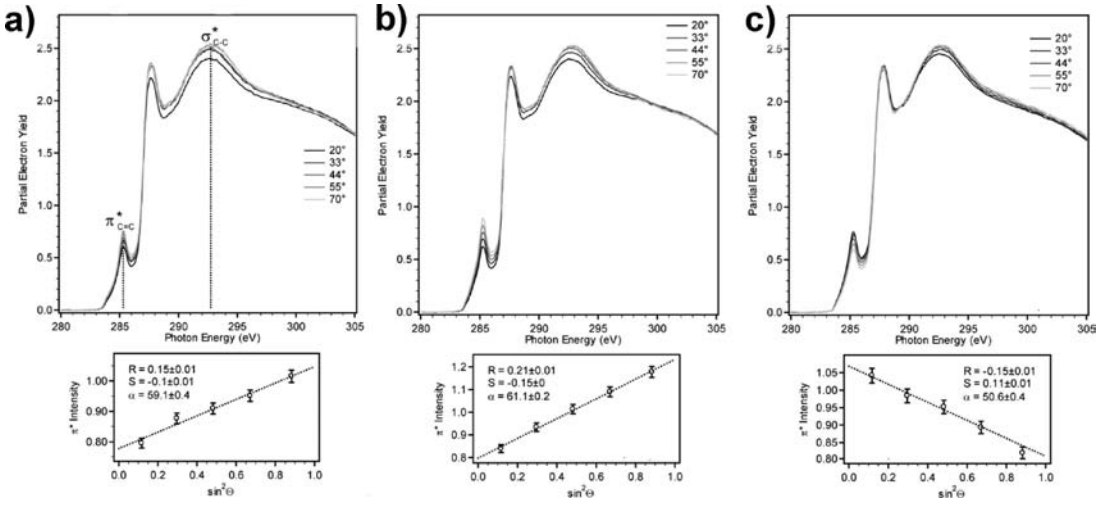

Figure 5. NEXAFS spectra acquired from the top interfaces of the polymer films: (a) DPPT-TT, as-cast; (b) DPPT-2T, annealed; and (c) DPPT-T, as-cast. NEXAFS partial electron yield has a standard uncertainty of ±2%. Photon energy has a standard uncertainty of ±0.1 eV.

reflected in the 1s → σ^* intensities, but it is complex to quantify, due to backbone contributions.

Figure 5 shows representative NEXAFS spectra acquired from the DPPT polymers. The carbon−carbon 1s → π^* and 1s → σ^* resonant excitation peaks appear at 285.3 and 292.8 eV, respectively, for all three polymers. The superimposed carbon−hydrogen and carbon−sulfur 1s → σ^* peaks appear at 287.6 eV for DPPT-TT and DPPT-2T, and shift slightly to 287.8 eV for DPPT-T. The spectra from DPPT-TT and DPPT-2T were very similar, with the greatest π^* intensities observed nearest normal incidence, while the spectra from DPPT-T showed the opposite. The figure of merit, R, was positive (0.15) for both as-cast DPPT-TT and DPPT-2T, but negative (−0.15) for as-cast DPPT-T (Table 3). These values were consistent with the molecular orientation inferred from GIXD patterns, indicating a preferentially edge-on orientation of the conjugated plane for as-cast DPPT-TT and DPPT-2T, and a preferentially face-on orientation for as-cast DPPT-T. In all three cases, thermal annealing resulted in more positive R values (0.22, 0.21, and 0.01, respectively), consistent with the reduced fraction of face-on domains as well as

Table 3. Dichroic ratios, R, for π^* Extracted from NEXAFS Spectra for Both Top and Bottom Interfaces of the DPPT Polymers

	top interface		bottom interface	
polymer	R, π^*, as-cast	R, π^*, annealed	R, π^*, as-cast	R, π^*, annealed
DPPT-TT	0.15 ± 0.01	0.22 ± 0.02	0.22 ± 0.02	0.20 ± 0.03
DPPT-2T	0.15 ± 0.01	0.21 ± 0.01	0.18 ± 0.04	0.19 ± 0.05
DPPT-T	-0.15 ± 0.01	0.01 ± 0.01	-0.20 ± 0.01	-0.11 ± 0.01

the improved orientation of edge-on domains seen in the GIXD patterns (Figure 4).

Charge transport occurs at semiconductor/dielectric interface in a BGBC transistor, and therefore, the molecular orientation at the bottom surface of the semiconductor film is the most relevant to TFT characteristics. To determine molecular orientation at the film bottom, films were delaminated using thin sheets of polydimethylsiloxane (PDMS) elastomer; we assume that the exposed interface is not modified by the delamination process.[38] NEXAFS can be used to confirm that no polymer remains on the substrate after delamination (see Figure S2 in the Supporting Information). For DPPT-TT and DPPT-2T, the R values obtained from the exposed bottom interfaces agreed reasonably well with those from the top interfaces (Table 3) and only changed slightly upon thermal annealing. For DPPT-T, the orientation of the conjugated plane was consistent on both sides of the as-cast films ($R = -0.15$ and -0.20 for top and bottom interfaces, respectively). However, after thermal annealing, the difference in R increased (0.01 and -0.11, respectively), with the top interface less face-on, or more disordered. This result suggests a mild vertical gradient in the average orientation that might be partially responsible for the difference in OTFT mobility between top gate and bottom gate DPPT-T devices (vide supra).

Variable Angle Spectroscopic Ellipsometry (VASE). VASE is a precise optical technique for determination of the dielectric properties (dielectric function or complex refractive index) of thin films.[4,34,39] In a typical measurement, the complex ratio of the amplitude reflectivity for the s (electric field perpendicular to the plane of incidence) and p (electric field in the plane of incidence) components of a reflected light beam are recorded as $\rho = r_p/r_s \equiv \tan \Psi\, e^{i\Delta}$. The two ellipsometric parameters, Ψ and Δ, are not associated directly with the physical properties of the thin film. They can be modeled by assuming that the sample is composed of a series of planar layers, with defined thickness and dielectric constant, on a similarly well-defined substrate. The best model whose calculated Ψ and Δ values fit the experimental data provides the optical constants and thickness values of the sample.

Shown in Figure 6 are the diagonal elements of the (assumed uniaxial) complex index of refraction ($n + ik$) for the three DPPT polymers. The best fit film thickness values were 31, 24, and 28 nm for DPPT-TT, DPPT-2T, and DPPT-T, respectively. All as-cast films are highly anisotropic, with the majority of the absorption due to the first strong singlet transition lying parallel to the substrate plane, indicating a strong preference for the polymer backbone to lie parallel to the substrate plane. The amount of residual absorption along the surface normal (z) increased monotonically across the series: DPPT-TT < DPPT-2T < DPPT-T. The ratio of the ε_{zz} and ε_{xx} components of the dielectric tensor ($\varepsilon \equiv \varepsilon' + i\varepsilon'' = (n + ik)^2$) can be related to the orientation average of the Euler angle θ representing the average tilt of the polymer long chain axis away from the surface normal.[34] The calculated θ values are 82°, 80°, and 76° for DPPT-TT, DPPT-2T, and DPPT-T, respectively. If one assumes that the film consists of a fraction, f, of material perfectly oriented in plane (with $\varepsilon''_{zz} = 0$) and a fraction $(1 - f)$ that is isotropic, then an estimate of f can be obtained based on the integral of ε'' over the entire absorption range.[34] With this approach, the f values were calculated to be 0.95 > 0.91 > 0.85 across the series: DPPT-TT > DPPT-2T > DPPT-T. We note that the as-cast DPPT-TT film is exceptionally anisotropic, with an f value even larger than that of PBTTT annealed from its mesophase ($f \approx 0.93$).[4] DPPT-2T is slightly less anisotropic than PBTTT. Although DPPT-T is the least anisotropic among the three polymers, it still exhibits an f value comparable to that of regioregular P3HT.[34,40] The dielectric functions of the annealed films are nominally identical with those of the as-cast films in terms of absorption edge and anisotropy. There is a slight decrease in total absorption upon annealing, possibly due to oxidation, and marginal change in anisotropy for all three polymers.

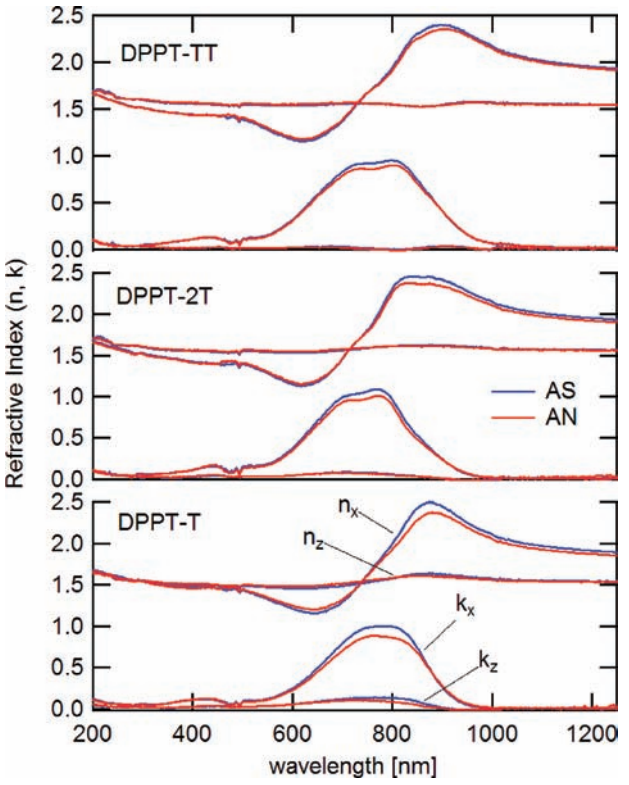

Figure 6. Complex indices of refraction for the DPPT polymers both parallel (x) and perpendicular to the surface plane (z). As-cast and annealed films are denoted as AS and AN, respectively.

Brewster's Angle Transmission Fourier Transform Infrared (FTIR) Spectroscopy. FTIR spectroscopy is capable of identifying structural information from individual moieties of the polymer

semiconductors, because certain vibrational resonances of these moieties can be detected independently.[26,34,40,41] For example, the side-chain methylene antisymmetrical stretch (ν_aCH_2) is typically observed between 2918 and 2928 cm^{-1}. Its actual peak position varies with the local structural order of the alkyl side chains; that is, the peak occurs near 2918 cm^{-1} for crystalline, all-trans configurations and shifts toward 2928 cm^{-1} for more disordered, liquidlike configurations.[26] For in-plane isotropic (uniaxial) films, the ratio of the *p*-polarized to *s*-polarized absorbance (A_p/A_s) of a band can be used to determine the average orientation of the relevant transition dipole with respect to the surface normal. Qualitatively, large A_p/A_s values correspond to dipoles oriented along the surface normal, while small A_p/A_s values correspond to those oriented in the surface plane.[40] The specific relationship requires knowledge of both the angle of the incidence and the index of the refraction of the film.

The vibrational resonances from the alkyl side chains and polymer backbone were identified in the DPPT polymer films (Figure 7 and Table 4). Note that the *p*-polarized data were rescaled to match the *s*-polarized in the CH_2 stretch region. In the 2800−3000 cm^{-1} region, the ν_aCH_2 frequencies for all three polymers (irrespective of thermal treatment) were found at ≈2924 cm^{-1}, indicating significant side chain disorder. The A_p/A_s values for these ν_aCH_2 bands (Table 4), as well as for the

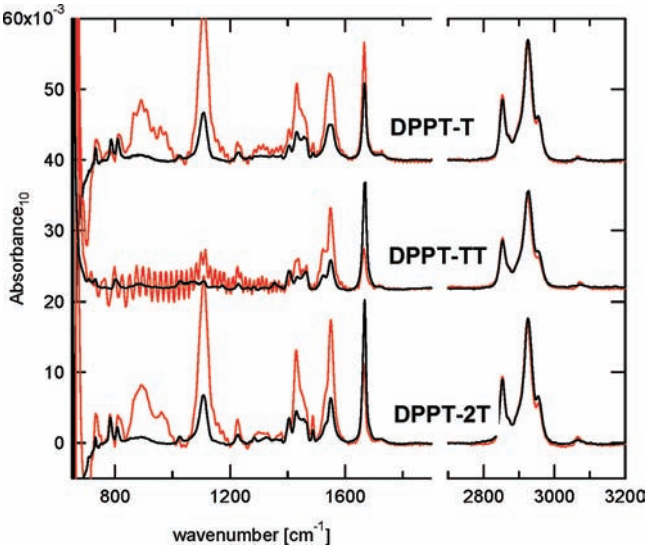

Figure 7. Polarized IR transmission spectra for as-cast DPPT polymer films, with the *s*-polarized spectra displayed in red and the *p*-polarized spectra in black.

ν_sCH_2 bands (methylene symmetrical stretch, peaking at ≈2853 cm^{-1}), were both determined to be ≈0.5, consistent with a nominally isotropic distribution of the methylenes.[34] In the fingerprint region of 1300−1600 cm^{-1}, the backbone stretching modes found at ≈1550, ≈ 1520, and ≈1487 cm^{-1} were assigned to C═C asymmetric stretches ($\nu_aC{=}C$) from DPP, TT, and 2T moieties, respectively. Quantum chemical calculations (performed with Gaussian 03) indicated that these C═C stretches were polarized nominally along the main-chain axis, and thus the low A_p/A_s values (≈ 0.20) for all three polymers reflect a strong in-plane orientation of the polymer main chains (Table 4). Assuming the IR index is bounded by the ordinary (1.56) and extraordinary (1.85) index of refraction measured in the near IR (1670 nm), the A_p/A_s is consistent with a long axis tilt of ≈80°, in good agreement with the more accurate visible VASE result. Moreover, there are strong C═O stretches observed at ≈1666−1667 cm^{-1} whose A_p/A_s values were high for as-cast DPPT-TT (1.42) and DPPT-2T (0.90), but low for as-cast DPPT-T (0.35). The A_p/A_s values all increased upon thermal annealing, to 1.57, 1.41, and 0.57 respectively (Table 3). Quantum chemical calculations helped to determine that the transition dipoles for the C═O asymmetric stretches ($\nu_aC{=}O$) were significantly tilted away from the main-chain axis (nominally 67° for both *syn* and *anti* forms). The observation of $A_p/A_s \approx$ 0.35 for as-cast DPPT-T indicates a majority face-on population; however, as the ratio is higher than observed for the C═C (nominally along the backbone), there must be some edge-on population, consistent with both the GIXD and NEXAFS results. The increase in A_p/A_s to 0.57 after annealing reflects the increase in the total edge-on population in the bimodal distribution. The large A_p/A_s values for DPPT-TT and DPPT-2T indicate preferential edge-on orientation of the conjugated planes.

Microscopic Measurements: Atomic Force Microscopy (AFM) and Dark-Field Transmission Electron Microscopy (DF-TEM). Tapping-mode AFM and dark-field TEM are techniques for visualizing the film in-plane texture. Whereas AFM probes the surface topography, DF-TEM can further map the orientation of a given director, for example, the $\pi-\pi$ stacking direction, provided that it is nominally constant through the thickness of the film.[42] The latter technique was recently established in our lab to map the in-plane crystal orientation of PBTTT films.[43] In that study, a series of DF images were acquired from a fixed area by allowing different portions of the isotropic (010) diffraction ring to transmit through a centered aperture positioned at the back focal plane of the objective lens. Subsequently, image analysis was used to extract the orientation information from the intensity patterns displayed by the DF image, ultimately

Table 4. Positions and A_p/A_s Ratios of Vibrational Resonances of DPPT Polymers Obtained from Transmission FTIR Spectra[a]

polymer	annealing condition	ν_sCH_2 (A_p/A_s)	ν_aCH_2 (A_p/A_s)	$\nu_aC{=}O$ (A_p/A_s)	$\nu_aC{=}C$ (A_p/A_s)	
DPPT-TT	as-cast	2853.1 (0.51)	2923.7 (0.52)	1666.2 (1.42)	1549.9 (0.21)	1522.5 (0.21)
	annealed	2853.4 (0.52)	2923.5 (0.52)	1666.8 (1.57)	1549.2 (0.20)	1520.4 (0.22)
DPPT-2T	as-cast	2853.2 (0.50)	2923.6 (0.49)	1665.8 (0.90)	1550.0 (0.20)	1487.0 (0.21)
	annealed	2853.2 (0.48)	2923.4 (0.50)	1667.1 (1.41)	1550.3 (0.20)	1486.6 (0.25)
DPPT-T	as-cast	2853.3 (0.49)	2923.9 (0.50)	1666.2 (0.35)	1549.2 (0.21)	1486.2 (0.08)
	annealed	2853.4 (0.55)	2923.9 (0.57)	1666.8(0.57)	1548.8 (0.24)	1486.8 (0.20)

[a] The standard deviation for the FTIR position is ±0.7 cm^{-1}, while the standard deviation for the A_p/A_s ratio is ±0.05, based on the pooled variance of multiple (two or three) spectra for most samples.

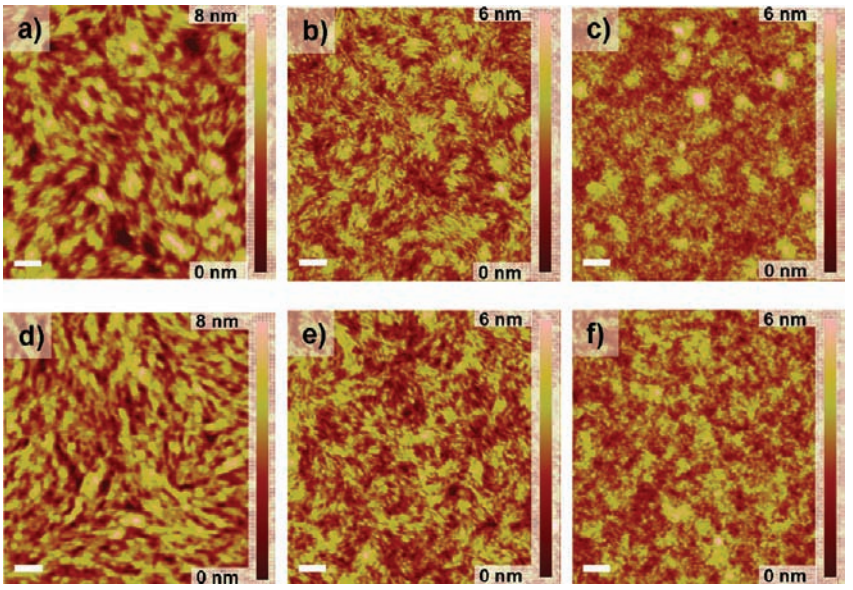

Figure 8. Tapping mode AFM height images of DPPT polymer films. (a) DPPT-TT, as-cast; (b) DPPT-2T, as-cast; (c) DPPT-T, as-cast; (d) DPPT-TT, annealed; (e) DPPT-2T, annealed; (f) DPPT-T, annealed. All scale bars denote 200 nm.

yielding a multicolor map with each color representing certain orientation range.[43]

For as-cast DPPT-TT and DPPT-2T films, fibrillar features were identified by AFM, with the width of the fibrils ≈30 nm for DPPT-TT and <20 nm for DPPT-2T (Figure 8a,b). The corresponding bright-field (BF) TEM images were both featureless (Figure S3 in the Supporting Information), consistent with the small variation of film thickness displayed in the AFM images. The significant contrast (bright domainlike features on dark backgrounds) in the DF images (Figure 9a,b) must therefore arise primarily from the variations of $\pi-\pi$ stacking direction. The $\pi-\pi$ stacking is responsible for the most intense electron diffraction ring, the (010), shown in the insets of Figure 9a,b. We note that the overall intensity of these diffraction patterns was quite weak compared to that of PBTTT with similar film thickness.[43] The existence of areas with common local orientation, which we will describe as "quasi-domains",[44] was verified by the appearance of a single pair of (010) arcs in diffraction patterns acquired from ≈300 nm diameter areas (Figure S4 in the Supporting Information), supporting the construction of multicolor orientation maps (Figure 9d,e). The characteristic length scales of the quasi-domains, calculated from the peak positions in the 2D power spectra of these orientation maps, were ≈1.2 μm and ≈500 nm for DPPT-TT and DPPT-2T (Figure 10a and d), respectively. Moreover, a gradient transition of quasi-domain orientations across the whole image, a trend found in PBTTT,[43,44] was also present in DPPT-TT and DPPT-2T. In other words, any given quasi-domain will find other quasi-domains with similar orientations in its vicinity. Although quasi-domains with large orientation differences are occasionally found in direct contact, such abrupt boundaries are bypassed by "bridging" quasi-domains with intermediate orientations. This gradient transition of the quasi-domain orientations reveals an in-plane liquid crystalline texture, which can be described quantitatively by a simple nearest neighbor analysis (Figure 10). Taking the orange pixels in Figure 9d as an example, the neighboring pixels are described in the orange curve in Figure 10c, where 80% of differently colored neighbors are red or yellow (denoted as R and Y, respectively, on the horizontal axis), titled by the lowest measurable angle away from the orange quasi-domains. Interestingly, this trend was also evident in the AFM images (Figure 8), as significant bends of the fibrils were not observed. Furthermore, by comparing DPPT-TT with DPPT-2T, it seemed that larger fibrils in AFM corresponded to larger quasi-domains in TEM, an observation similar to that of the terrace size versus quasi-domain size in PBTTT.[43]

For an as-cast DPPT-T film, fibrillar features were barely discernible in its AFM image, and the whole film appeared nodule-like (Figure 8c). The (010) diffraction ring could not be discerned in the electron diffraction pattern (inset of Figure 9c), most likely due to the orthogonality of out-of-plane $\pi-\pi$ stacking and the in-plane scattering vector of the electron beam. Consequently, the contrast in its DF images (Figure 9c) was insufficient for constructing an orientation map. In addition, while the effect of thermal annealing was evident in the spectroscopic measurements for the DPPT polymers, it was not apparent in AFM and TEM measurements (Figure 8d–f and Supporting Information Figure S5).

DISCUSSION

The Effect of Backbone Organization on OTFT Device Performance. The detailed measurements of molecular packing described above agree reasonably well, pointing to a general behavior that is schematically depicted in Figure 11. The molecular packing behaviors of DPPT-TT and DPPT-2T closely resemble each other (Figure 11a,b), showing a "classic" lamellar packing motif with edge-on conjugated planes of the backbone. The minor face-on chains in the as-cast films could be reoriented with brief thermal treatment. The difference in characteristic quasi-domain length scale between DPPT-TT and DPPT-2T is more than twofold (revealed by DF-TEM), which likely originates from the increased backbone rigidity of DPPT-TT. However, the large quasi-domain size of DPPT-TT does not lead to remarkably increased μ_{sat} values in long-channel OTFT devices compared with DPPT-2T. Such insensitivity of mobility to quasi-domain size could be explained by the low density of abrupt grain

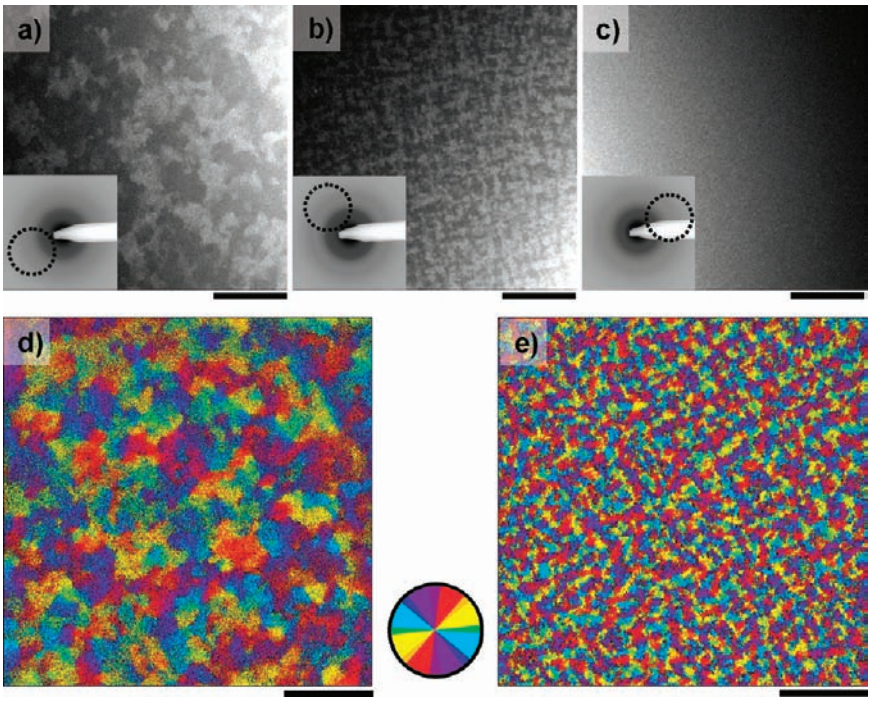

Figure 9. Dark-field TEM images of as-cast films of (a) DPPT-TT; (b) DPPT-2T; and (c) DPPT-T, and corresponding orientation maps of (d) DPPT-TT and (e) DPPT-2T. The insets of the dark-field TEM images show the diffraction patterns acquired from the same areas and illustrate the beam-tilt configurations for image acquisition. Note that the objective aperture (dashed circle) is always centered in the TEM column. The color wheel between the orientation maps shows the correlation of the colors with $\pi-\pi$ stacking directions. All scale bars denote 2 μm.

boundaries in both DPPT-TT and DPPT-2T (Figures 9d,e and 10): the local change of orientation within a quasi-domain or across adjacent two quasi-domains is modest, ensuring the formation of percolative pathways across the length of an OTFT channel, irrespective of the quasi-domain size. A similar effect has also been observed in PBTTT films where changes in quasi-domain size with casting solvent were not strongly correlated to mobility.[43] While the difference in quasi-domain size was only $\approx$1.5 times between PBTTT films processed from different solvents, it is larger here (2.5 times), further supporting the conjecture that the local distribution of polymer orientation may ultimately dominate charge transport processes.[43] Thermal annealing does not lead to noticeable change in domain size, suggesting the absence of mesophases within the annealing temperature range that we used,[45] which could be corroborated by thermal analysis of DPPT-TT reported by Li et al.[20] and the unchanged texture in in situ observation from room temperature to 180 °C under cross-polarized optical microscope (Figure S6 in the Supporting Information).

The backbone organization of an as-cast DPPT-T film is remarkably different from the other two DPPT derivatives, with preferentially face-on orientation of the conjugated plane (Figure 11c), more closely resembling the molecular packing behavior of the previously reported P(NDI2OD-T2)[12] and IDT-BT.[19] The μ_{sat} values of as-cast DPPT-T are adequately high for logic circuit applications,[46] though the device performance of long-channel bottom gate bottom contact devices is 50−70% lower compared to those of DPPT-TT and DPPT-2T. The structure−property relationship of DPPT-T can be discussed by combining two arguments: (1) Charge transport along the polymer backbone is 1−2 orders of magnitude faster than that along the $\pi-\pi$ direction, as demonstrated by both experiment and theoretical calculation.[47,48] (2) As suggested by Rivnay et al.,[12] the electric field distribution in a transistor should allow charge carriers to populate at least 2−3 molecular layers adjacent to the semiconductor/dielectric interface for face-on molecules, in contrast to the monolayer charge population for edge-on molecules. Given these premises, charge transport is expected to occur primarily along the polymer backbone, and charge hopping to an adjacent chain via interchain $\pi-\pi$ stacking only occurs when the conjugation is interrupted. Whereas edge-on backbone orientation allows in-plane interchain charge hopping, face-on backbone orientation may also allow effective out-of-plane interchain charge hopping within the 2−3 molecular layers nearest to the bottom interface. Therefore, a highly anisotropic polymer film such as DPPT-T, with its long chain axis lying parallel to the surface plane as revealed by our VASE measurements, can be capable of high field-effect mobility. Moreover, we speculate that the higher field-effect mobilities obtained from DPPT-TT and DPPT-2T might originate from their stronger long axis orientation and their in-plane liquid crystalline texture, not necessarily their edge-on conjugated plane orientation. A robust comparison of device performance between the edge-on and face-on DPPT-T, unfortunately, has not been possible, since the edge-on packing is not "pure" in annealed DPPT-T films, and the overall degree of order is dissimilar for the edge-on and face-on components. Nevertheless, further studies on changes in molecular packing behavior by altering processing parameters may facilitate such a comparison.

The strong preference for in-plane order of the long chain axis might arise from remarkable backbone rigidity or coplanarization. In this regard, UV−vis−NIR absorption spectroscopy can provide useful information, as red shifts of the absorption peak position have been related to enhancement of effective backbone

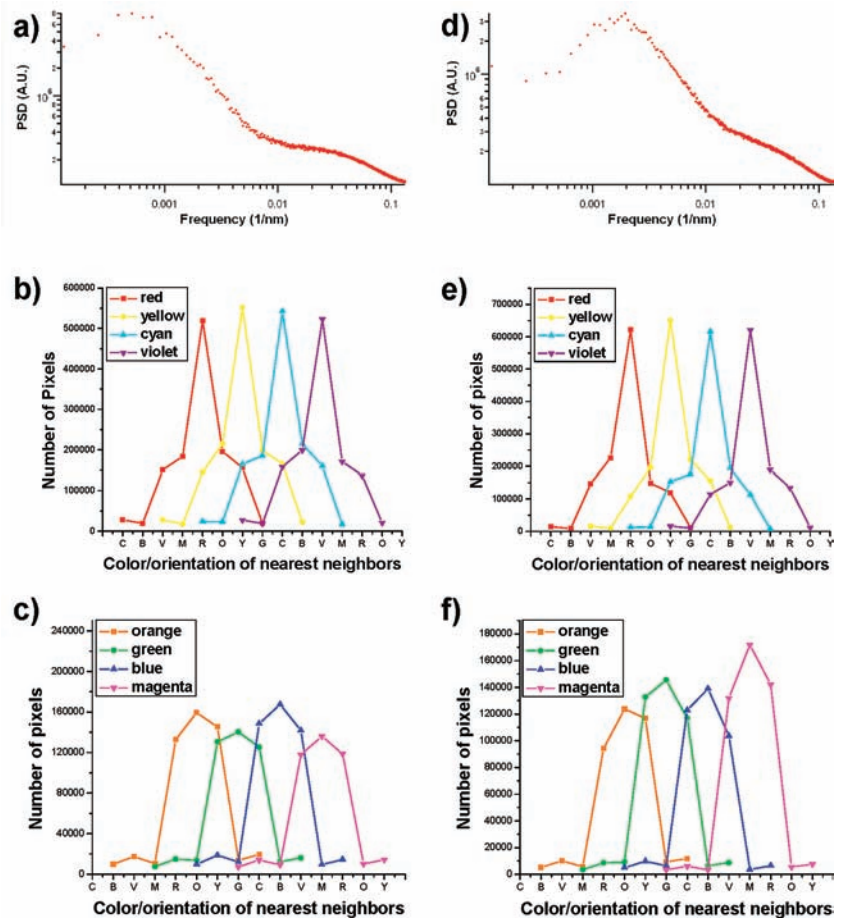

Figure 10. Power spectra and neighborhood analysis curves acquired from Figure 8d and 8e. (a–c) and (d–f) correspond to as-cast films of DPPT-TT and DPPT-2T, respectively.

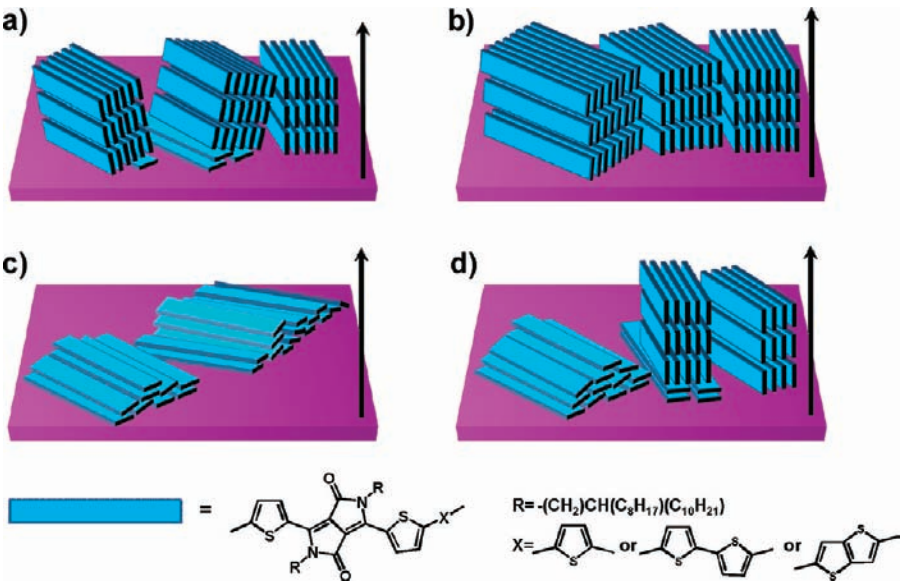

Figure 11. Illustrations for the molecular packing motifs in (a) as-cast DPPT-TT and DPPT-2T films; (b) annealed DPPT-TT and DPPT-2T films; (c) as-cast DPPT-T film; and (d) annealed DPPT-T film. The arrows denote the film surface normal direction.

conjugation length by greater ring coplanarity.[49,50] Regioregular P3HT, a well-known example, displays an ≈100 nm shift from solution to thin film.[50] In contrast, this shift is no larger than ≈20 nm for the DPPT polymers (Table 2 and Figure 12). Moreover, thermal

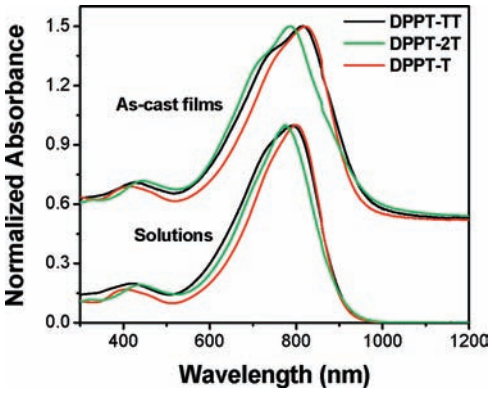

Figure 12. Normalized UV−vis-NIR absorption spectra of DPPT-TT, DPPT-2T, and DPPT-T for both solutions in chloroform and as-cast films. For ease of comparison, the film spectra are elevated by 0.5 absorbance units.

annealing resulted in only marginal changes in DPPT-TT and DPPT-2T film spectra (somewhat larger in DPPT-T, ≈ 8 nm, Table 2). Studies of oligomers with a DPPT-2T-like repeat, but with additional side chains on the thiophenes, demonstrate significantly blue-shifted absorption for twisted conformations in solution.[51] Therefore, both the solution and film of the polymers studied here have a rigid chain conformation where the rings are highly coplanar. A highly coplanar backbone is consistent with the excellent OTFT device performance. The strong tendency for planarization likely arises from both the extended π-planes and additional chain−chain interactions arising from the donor−acceptor motif.

The Impact of Bulky Side Chain on Backbone Organization. It is important to question why the backbone packing motif of DPPT-T is significantly different from that of DPPT-TT and DPPT-2T. We hypothesize that the variation in attachment density of the branched alkyl side chains is responsible for this difference in molecular packing behavior. To support this hypothesis, we include the previously reported P(NDI2OD-T2)[11,12] in the following comparison, since it possesses the same side chains (2-octyldodecyl groups) as those of the DPPT polymers. The repeat unit length (estimated from molecular mechanics calculations) decreases in the sequence of DPPT-2T (1.97 nm), DPPT-TT (1.80 nm), DPPT-T (1.58 nm), and P(NDI2OD-T2) (1.44 nm), inversely proportional to an increasing 2D side-chain attachment density since the $\pi-\pi$ stacking distance is similar. Correspondingly, the packing behavior shows a transition from edge-on packing to bimodal distribution to face-on packing. The mechanism by which the attachment density influences the orientation is currently unclear. However, for well-ordered lamella, as are observed for DPPT-TT and DPPT-2T, one would expect the lowest free energy simple crystal face to be the (100) alkyl-terminated plane with the π-terminated (010) plane slightly higher in energy. At a low free energy surface such as the OTS treated dielectric, edge-on packing should be the lowest energy configuration. This suggests that the face-on configuration for DPPT-T is a kinetically created metastable state, consistent with the decrease in face-on population upon annealing. We note that P(NDI2OD-T2) also adopts an edge-on orientation when slowly cooled from the melt.[52] It is expected that the bulky side groups will hinder the development of $\pi-\pi$ stacking for the polymers with high side chain attachment densities. This may slow the development of well-formed lamella and facilitate metastable state formation. In the absence of lamella, the face-on orientation should be energetically favorable due to increased dispersion interaction with the π-system. This is supported by the vertical gradient observed in NEXAFS for DPPT-T; the face-on orientation is more persistent at the substrate interface.

CONCLUSIONS

Our studies of the molecular packing behavior of DPP-based semiconducting polymers revealed extraordinary in-plane orientation of the polymer main chains, irrespective of whether the conjugated plane was edge-on or face-on. We suggest that this structural characteristic, together with the closely correlated local ring coplanarity, is primarily responsible for their excellent OTFT device performance. The in-plane liquid-crystal-like texture, like that found in PBTTT,[43] may also contribute to the high field-effect mobilities. Organization of the conjugated backbone is not necessarily interrupted by the disordered, bulky side chains. Donor−acceptor copolymers with branched side chains, such as the DPPT polymers discussed in this Article, may represent an important trend in designing future materials for OTFT and relevant applications, due to their excellent solution processability with uncompromised device performance.

ASSOCIATED CONTENT

Supporting Information. Additional tables and figures about transistor performance, diffraction, and spectroscopic and microscopic characterization. This material is available free of charge via the Internet at http://pubs.acs.org.

AUTHOR INFORMATION

Corresponding Author
dean.delongchamp@nist.gov; i.mcculloch@imperial.ac.uk

ACKNOWLEDGMENT

The authors thank Dr. C. R. Snyder and Dr. S. D. Hudson for valuable discussions. X. Z. thanks Dr. B. R. Conrad and Dr. C. K. Chan for fabricating Pt-based bottom gate bottom contact transistor test beds. X. Z. also thanks Dr. D. S. Germack for his assistance in VASE and FTIR measurements. The synthesis of all polymers was in part carried out under the EC FP7 ONE-P Project Number 212311 and DPI Grant 678, with support from the international collaborative research program of Gyeonggi-do, Korea. Portions of this research were carried out at the Stanford Synchrotron Radiation Laboratory, a national user facility operated by Stanford University on behalf of the U.S. Department of Energy, Office of Basic Energy Sciences.

REFERENCES

(1) Sirringhaus, H.; Brown, P. J.; Friend, R. H.; Nielsen, M. M.; Bechgaard, K.; Langeveld-Voss, B. M. W.; Spiering, A. J. H.; Janssen, R. A. J.; Meijer, E. W.; Herwig, P.; de Leeuw, D. M. *Nature* **1999**, *401*, 685.

(2) Ong, B. S.; Wu, Y. L.; Liu, P.; Gardner, S. *J. Am. Chem. Soc.* **2004**, *126*, 3378.

(3) McCulloch, I.; Heeney, M.; Bailey, C.; Genevicius, K.; Macdonald, I.; Shkunov, M.; Sparrowe, D.; Tierney, S.; Wagner, R.; Zhang, W. M.; Chabinyc, M. L.; Kline, R. J.; McGehee, M. D.; Toney, M. F. *Nat. Mater.* **2006**, *5*, 328.

(4) DeLongchamp, D. M.; Kline, R. J.; Lin, E. K.; Fischer, D. A.; Richter, L. J.; Lucas, L. A.; Heeney, M.; McCulloch, I.; Northrup, J. E. *Adv. Mater.* **2007**, *19*, 833.
(5) McCulloch, I.; et al. *Adv. Mater.* **2009**, *21*, 1091.
(6) Burgi, L.; Turbiez, M.; Pfeiffer, R.; Bienewald, F.; Kirner, H. J.; Winnewisser, C. *Adv. Mater.* **2008**, *20*, 2217.
(7) Liu, J. Y.; Zhang, R.; Sauve, G.; Kowalewski, T.; McCullough, R. D. *J. Am. Chem. Soc.* **2008**, *130*, 13167.
(8) Osaka, I.; Zhang, R.; Sauve, G.; Smilgies, D. M.; Kowalewski, T.; McCullough, R. D. *J. Am. Chem. Soc.* **2009**, *131*, 2521.
(9) Osaka, I.; Abe, T.; Shinamura, S.; Miyazaki, E.; Takimiya, K. *J. Am. Chem. Soc.* **2010**, *132*, 5000.
(10) Osaka, I.; Zhang, R.; Liu, J.; Smilgies, D.-M.; Kowalewski, T.; McCullough, R. D. *Chem. Mater.* **2010**, *22*, 4191.
(11) Yan, H.; Chen, Z. H.; Zheng, Y.; Newman, C.; Quinn, J. R.; Dotz, F.; Kastler, M.; Facchetti, A. *Nature* **2009**, *457*, 679.
(12) Rivnay, J.; Toney, M. F.; Zheng, Y.; Kauvar, I. V.; Chen, Z.; Wagner, V.; Facchetti, A.; Salleo, A. *Adv. Mater.* **2010**, *22*, 4359.
(13) Zhang, M.; Tsao, H. N.; Pisula, W.; Yang, C. D.; Mishra, A. K.; Mullen, K. *J. Am. Chem. Soc.* **2007**, *129*, 3472.
(14) Tsao, H. N.; Cho, D.; Andreasen, J. W.; Rouhanipour, A.; Breiby, D. W.; Pisula, W.; Mullen, K. *Adv. Mater.* **2009**, *21*, 209.
(15) Kim, D. H.; Lee, B. L.; Moon, H.; Kang, H. M.; Jeong, E. J.; Park, J. I.; Han, K. M.; Lee, S.; Yoo, B. W.; Koo, B. W.; Kim, J. Y.; Lee, W. H.; Cho, K.; Becerril, H. A.; Bao, Z. *J. Am. Chem. Soc.* **2009**, *131*, 6124.
(16) Guo, X. G.; Kim, F. S.; Jenekhe, S. A.; Watson, M. D. *J. Am. Chem. Soc.* **2009**, *131*, 7206.
(17) Mondal, R.; Miyaki, N.; Becerril, H. A.; Norton, J. E.; Parmer, J.; Mayer, A. C.; Tang, M. L.; Bredas, J. L.; McGehee, M. D.; Bao, Z. A. *Chem. Mater.* **2009**, *21*, 3618.
(18) Di, C. A.; Lu, K.; Zhang, L.; Liu, Y. Q.; Guo, Y. L.; Sun, X. N.; Wen, Y. G.; Yu, G.; Zhu, D. B. *Adv. Mater.* **2010**, *22*, 1273.
(19) Zhang, W.; Smith, J.; Watkins, S. E.; Gysel, R.; McGehee, M.; Salleo, A.; Kirkpatrick, J.; Ashraf, S.; Anthopoulos, T.; Heeney, M.; McCulloch, I. *J. Am. Chem. Soc.* **2010**, *132*, 11437.
(20) Li, Y. N.; Singh, S. P.; Sonar, P. *Adv. Mater.* **2010**, *22*, 4862.
(21) Sonar, P.; Singh, S. P.; Li, Y.; Soh, M. S.; Dodabalapur, A. *Adv. Mater.* **2010**, *22*, 5409.
(22) Bronstein, H.; et al. *J. Am. Chem. Soc.* **2011**, *133*, 3272.
(23) Tsao, H. N.; Cho, D. M.; Park, I.; Hansen, M. R.; Mavrinskiy, A.; Yoon, D. Y.; Graf, R.; Pisula, W.; Spiess, H. W.; Mullen, K. *J. Am. Chem. Soc.* **2011**, *133*, 2605.
(24) Huitema, H. E. A.; Gelinck, G. H.; van der Putten, J.; Kuijk, K. E.; Hart, K. M.; Cantatore, E.; de Leeuw, D. M. *Adv. Mater.* **2002**, *14*, 1201.
(25) Steudel, S.; Myny, K.; Arkhipov, V.; Deibel, C.; De Vusser, S.; Genoe, J.; Heremans, P. *Nat. Mater.* **2005**, *4*, 597.
(26) Kline, R. J.; DeLongchamp, D. M.; Fischer, D. A.; Lin, E. K.; Richter, L. J.; Chabinyc, M. L.; Toney, M. F.; Heeney, M.; McCulloch, I. *Macromolecules* **2007**, *40*, 7960.
(27) Baklar, M.; Wobkenberg, P. H.; Sparrowe, D.; Goncalves, M.; McCulloch, I.; Heeney, M.; Anthopoulos, T.; Stingelin, N. *J. Mater. Chem.* **2010**, *20*, 1927.
(28) Sirringhaus, H.; Kawase, T.; Friend, R. H.; Shimoda, T.; Inbasekaran, M.; Wu, W.; Woo, E. P. *Science* **2000**, *290*, 2123.
(29) Arias, A. C.; MacKenzie, J. D.; McCulloch, I.; Rivnay, J.; Salleo, A. *Chem. Rev.* 2010, *110*, 3.
(30) Tekin, E.; Smith, P. J.; Schubert, U. S. *Soft Matter* **2008**, *4*, 703.
(31) Kline, R. J.; McGehee, M. D.; Kadnikova, E. N.; Liu, J. S.; Frechet, J. M. J.; Toney, M. F. *Macromolecules* **2005**, *38*, 3312.
(32) Hamadani, B. H.; Gundlach, D. J.; McCulloch, I.; Heeney, M. *Appl. Phys. Lett.* **2007**, *91*, 243512.
(33) Chabinyc, M. L.; Toney, M. F.; Kline, R. J.; McCulloch, I.; Heeney, M. *J. Am. Chem. Soc.* **2007**, *129*, 3226.
(34) DeLongchamp, D. M.; Kline, R. J.; Fischer, D. A.; Richter, L. J.; Toney, M. F. *Adv. Mater.* **2011**, *23*, 319.
(35) Prosa, T. J.; Winokur, M. J.; Moulton, J.; Smith, P.; Heeger, A. J. *Macromolecules* **1992**, *25*, 4364.
(36) Stöhr, J. *NEXAFS Spectroscopy*; Spinger-Verlag: Berlin, 1992.
(37) DeLongchamp, D. M.; Vogel, B. M.; Jung, Y.; Gurau, M. C.; Richter, C. A.; Kirillov, O. A.; Obrzut, J.; Fischer, D. A.; Sambasivan, S.; Richter, L. J.; Lin, E. K. *Chem. Mater.* **2005**, *17*, 5610.
(38) Chabinyc, M. L.; Salleo, A.; Wu, Y. L.; Liu, P.; Ong, B. S.; Heeney, M.; McCulloch, I. *J. Am. Chem. Soc.* **2004**, *126*, 13928.
(39) Tammer, M.; Monkman, A. P. *Adv. Mater.* **2002**, *14*, 210.
(40) Gurau, M. C.; Delongchamp, D. M.; Vogel, B. M.; Lin, E. K.; Fischer, D. A.; Sambasivan, S.; Richter, L. J. *Langmuir* **2007**, *23*, 834.
(41) DeLongchamp, D. M.; Kline, R. J.; Jung, Y.; Lin, E. K.; Fischer, D. A.; Gundlach, D. J.; Cotts, S. K.; Moad, A. J.; Richter, L. J.; Toney, M. F.; Heeney, M.; McCulloch, I. *Macromolecules* **2008**, *41*, 5709.
(42) Williams, D. B.; Carter, C. B. *Transmisson Electron Microscopy*; Plenum Press: New York, 1996.
(43) Zhang, X.; Hudson, S. D.; DeLongchamp, D. M.; Gundlach, D. J.; Heeney, M.; McCulloch, I. *Adv. Funct. Mater.* **2010**, *20*, 4098.
(44) The term "quasi-domain" used here refers to a region within which the polymer chains are similarly oriented. It is somewhat different from the conventional concept of a crystalline domain, as the observed size and shape of a quasi-domain greatly depends on how the beam-tilt configuration is defined.
(45) Pisula, W.; Zorn, M.; Chang, J. Y.; Mullen, K.; Zentel, R. *Macromol. Rapid Commun.* **2009**, *30*, 1179.
(46) Bijleveld, J. C.; Zoombelt, A. P.; Mathijssen, S. G. J.; Wienk, M. M.; Turbiez, M.; de Leeuw, D. M.; Janssen, R. A. J. *J. Am. Chem. Soc.* **2009**, *131*, 16616.
(47) Street, R. A.; Northrup, J. E.; Salleo, A. *Phys. Rev. B* **2005**, 71.
(48) Lan, Y. K.; Huang, C. I. *J. Phys. Chem. B* **2009**, *113*, 14555.
(49) McCullough, R. D.; Lowe, R. D.; Jayaraman, M.; Anderson, D. L. *J. Org. Chem.* **1993**, *58*, 904.
(50) Chen, T. A.; Wu, X. M.; Rieke, R. D. *J. Am. Chem. Soc.* **1995**, *117*, 233.
(51) Karsten, B. P.; Janssen, R. A. J. *Macromol. Chem. Phys.* **2011**, *212*, 515.
(52) Rivnay, J.; Steyrleuthner, R.; Jimison, L. H.; Casadei, A.; Chen, Z.; Toney, M. F.; Facchetti, A.; Neher, D.; Salleo, A. *Macromolecules* **2011**, *44*, 5246.